Journal of Power Sources 195 (2010) 3256–3260

Contents lists available at ScienceDirect

Journal of Power Sources

journal homepage: www.elsevier.com/locate/jpowsour

Short communication

Evaluation of electrodeposited Fe–Ni alloy on ferritic stainless steel solid oxide fuel cell interconnect

Shujiang Geng[a,*], Yandong Li[a], Zhonghe Ma[a], Linlin Wang[a], Linna Li[a], Fuhui Wang[b]

[a] School of Materials and Metallurgy, Box 119, Northeastern University, 3-11 Wenhua Road, Shenyang 110004, China
[b] State Key Laboratory for Corrosion and Protection, Institute of Metal Research, Chinese Academy of Sciences, 62 Wencui Road, Shenyang 110016, China

ARTICLE INFO

Article history:
Received 11 November 2009
Received in revised form 1 December 2009
Accepted 2 December 2009
Available online 5 December 2009

Keywords:
Solid oxide fuel cell
Fe–Ni alloy
Interconnect
Oxidation
Area specific resistance

ABSTRACT

Fe–Ni alloy is electrodeposited on ferritic stainless steel for intermediate-temperature solid oxide fuel cell (SOFC) interconnects application. The oxidation behavior of Fe–Ni alloy coated steel has been investigated at 800 °C in air corresponding to the cathode environment of SOFC. It is found that the oxidation rate of the Fe–Ni alloy coated steel becomes similar to that of the uncoated steel after the first week thermal exposure, although the mass gain of the coated steel is higher than that of the uncoated steel. Oxide scale formed on the uncoated steel mainly consists of Cr_2O_3 with $(Mn,Cr)_3O_4$ spinel. However, a double-layer oxide structure with a Cr-free outer layer of $Fe_2O_3/NiFe_2O_4$ and an inner layer of Cr_2O_3 is developed on the Fe–Ni alloy coated steel. The scale area specific resistance (ASR) for the Fe–Ni alloy coated steel is lower than that of the scale for the uncoated steel.

1. Introduction

Solid oxide fuel cells (SOFCs) are electrochemical devices that directly convert chemical energy from fossil fuel into electricity [1]. They have received a great deal of attention due to their advantages such as low emission, fuel flexibility and high efficiency. However, some major technical hurdles related to materials must be overcome in order to commercialize SOFC technologies [2–4]. One of them is interconnect materials that connect individual cells into electrical series in a cell stack and separate fuel and oxidant gases. In order to perform their intended functions, the interconnects must fulfill some stringent criteria [5] such as a match in coefficient of thermal expansion (CTE) with other cell components, stability in both oxidizing and reducing atmospheres at the operating temperature, high electronic and thermal conductivity, chemical compatibility with both anode and cathode materials.

With the reduction in SOFC operating temperatures to the range of 600–800 °C [6–9], it is possible to employ cost-effective high temperature oxidation resistant alloys as SOFC interconnects to supplant the conventional $LaCrO_3$-based ceramics which suffer from high expense and difficulties in fabrication. Ferritic stainless steels are among the most promising candidates for SOFC interconnects due to their electrically conductive oxide scale, good mechanical properties, ease of fabrication, low cost and thermal expansion match with other cell components [2,10–15]. However, one challenge associated with ferritic stainless steel is the migration of chromium via chromia scale evaporation. Volatile Cr species from chromia scale can migrate to and poison the cathode or the interface between cathode and electrolyte [16,17], leading to the degradation of SOFC performance [18–23]. To solve the problem, some coatings have been developed on ferritic stainless steels. Especially, Cr-free coatings are highly desirable to hinder the vaporization of chromia scale. Perovskite coatings such as slurry-coated $(La,Sr)MnO_3$ [24], spin-coated or electron beam physical vapor deposited $(La,Sr)CoO_3$ [25] and radio frequency sputtered $(La,Sr)FeO_3$ [26,27] oxide coatings on Fe–Cr alloys were evaluated for intermediate-temperature SOFC interconnects application. In addition to perovskite coatings, Mn–Co spinel oxides [28–31] were investigated as an electrically conductive and protective coating on ferritic stainless steels. They appear to be effective in mitigating chromium migration and minimizing surface oxides scale area specific resistance.

Previous research indicated that $(Fe,Ni)_3O_4$ spinel layer thermally grown on Fe–Ni alloys in SOFC cathode environment had a high electrical conductivity and CTE match with other cell components [32]. In this study, Fe–Ni alloy is deposited on the ferritic stainless steel using the cost-effective technique of electrodepositing, followed by thermal exposure in typical SOFC cathode operating environment. It is expected that the Fe–Ni alloy layer can be converted into a $(Fe,Ni)_3O_4$ spinel layer which covers the chromium oxide formed from the steel substrate. The oxidation behavior of the coated steel in air at 800 °C is investigated and

* Corresponding author. Tel.: +86 24 83673860; fax: +86 24 83687731.
E-mail address: gengsj@smm.neu.edu.cn (S. Geng).

0378-7753/$ – see front matter © 2009 Elsevier B.V. All rights reserved.
doi:10.1016/j.jpowsour.2009.12.007

the electrical resistance of the oxide scale thermally grown on the coated steel is measured. The potential of the Fe–Ni alloy as SOFC interconnects coating will be discussed.

2. Experimental

2.1. Electrodeposition

Rectangular coupons of 15 mm × 10 mm × 1.0 mm were cut from the ferritic stainless steel sheet (nominal weight percent: 16.4% Cr, 0.28% Si, 0.13% Mn, 0.005% P, 0.005% C, 0.004% S, and the balance Fe) by electric-discharge machining (EDM). After drilling a 1.5-mm diameter hole in the upper center, each coupon was ground to 1000 grits with SiC sand paper, ultrasonically cleaned in acetone, followed by rinsing in alkaline and acid solutions, respectively, and then electrodeposited in the solution with pH value adjusted to 3.5, containing 40 g L^{-1} $NiSO_4{\cdot}6H_2O$, 5 g L^{-1} $NiCl_2{\cdot}6H_2O$, 20 g L^{-1} $FeSO_4{\cdot}7H_2O$ and 10 g L^{-1} H_3BO_3. The stainless steel substrate was used as the cathode and nickel plate was used as the anode. The experimental procedure was carried out as described recently [33]. Fe–Ni alloy was electrodeposited at 60 °C under a cathode current density of 27 mA cm^{-2} for 5 min, resulting in an around 3.0 μm thick Fe–Ni alloy coating on the steel surface as shown in the next discussion.

2.2. Oxidation testing

Oxidation testing of the Fe–Ni alloy coated and uncoated steels were conducted in a box furnace. The coupons were hung in alumina crucibles, oxidized at 800 °C in air for totally 3 weeks. The weight of each coupon was measured after furnace cooling to room temperature following each 1-week thermal exposure. The phase structures of the oxide scales formed on the coupons were identified with X-ray diffraction (XRD). The surface morphologies and cross-sections of the oxidized coupons were observed using scanning electron microscopy (SEM) with an energy dispersive X-ray spectroscopy (EDX).

2.3. Scale area specific resistance measurement

Electrical resistance of oxidized coupons was measured using 4-point method from 600 to 800 °C in air. The measurement apparatus was design as shown in Fig. 1. Two of the oxidized surfaces were covered with Pt paste. Each Pt foil had two welded Pt leads. Two alumina rods and springs were used to apply pressure and clamp the assembly together during measurement. One pair of leads was used to apply a constant current and the other pair was for voltage measurement. A constant current of 10 mA was used in the measurement reported in this paper. At each temperature, the resistance (R) was calculated according to the Ohm's law, $R = V/2I$.

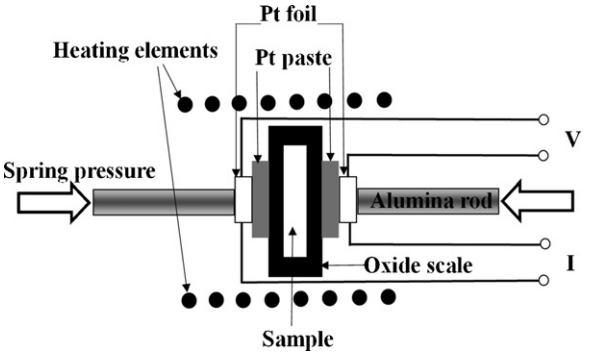

Fig. 1. Schematic apparatus for oxide scale area specific resistance measurement.

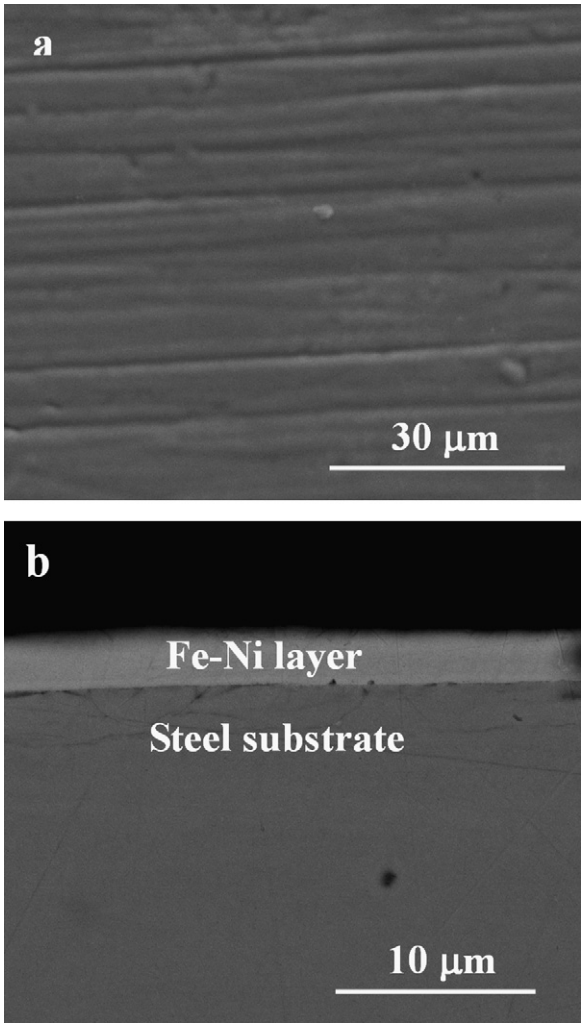

Fig. 2. SEM surface (a) and cross-section (b) images of as-electrodeposited Fe–Ni alloy on ferritic stainless steel.

The area specific resistance (ASR) of the oxide scales which reflected both the electrical conductivity and the thickness of the oxide scale was then equal to R multiplied by the area that the Pt paste covered.

3. Results and discussion

3.1. Morphologies and phase structure of as-electrodeposited Fe–Ni alloy

Fig. 2 shows the surface and cross-section morphologies of the Fe–Ni layer coated ferritic stainless steel. The electrodeposited Fe–Ni layer was continuous and dense with an average thickness of about 3.0 μm, and was well bonded to the steel substrate. Analysis by EDX indicated that Fe and Ni contents in the Fe–Ni layer was 41.7 and 58.3 wt.%, respectively. The composition of the as-electrodeposited Fe–Ni layer was close to that of Fe–60 wt.% Ni alloy on which $(Fe,Ni)_3O_4$ spinel oxide was mainly formed after thermal exposure in air at 800 °C [32]. The phase structure of the electrodeposited Fe–Ni layer was comprised of Fe–Ni alloy with preferred orientations of (1 1 1) and (2 0 0) as shown in Fig. 3, which is consistent with that reported in recent study [33]. It is obvious that Fe–Ni alloy layer has been successfully electrodeposited on the ferritic stainless steel.

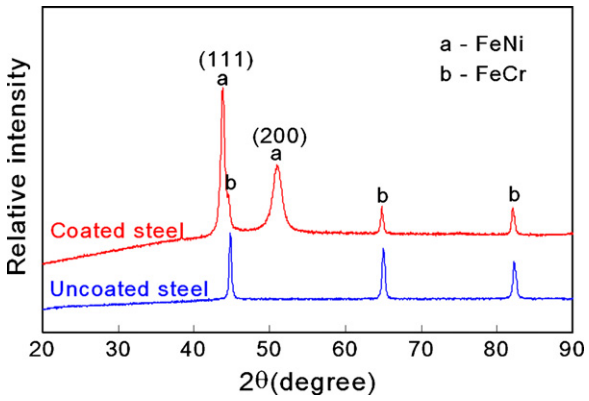

Fig. 3. XRD patterns of Fe–Ni alloy coated and uncoated steels.

3.2. Oxidation behaviors

The oxidation kinetics of the Fe–Ni alloy coated steel in air at 800 °C was compared with that of the uncoated steel. Their specific mass changes as a function of oxidation time are shown in Fig. 4. The coated steel experienced an initially large specific mass gain, followed by a transition to slower oxidation kinetics similar to that of the uncoated steel after the first-week thermal exposure, implying a protective oxide scale formation between the substrate and the surface oxides developed during the initial rapid oxidation stage.

Fig. 5 shows XRD patterns for oxidized coupons in air at 800 °C. The oxide scale formed on the uncoated steel after a 3-week oxidation consisted of Cr_2O_3 and $(Mn,Cr)_3O_4$, consistent with the phase structure of surface oxide scale developed on Fe–Cr–Mn ferritic steel [11]. However, the oxides including $NiFe_2O_4$, Cr_2O_3 and Fe_2O_3 were thermally grown on the coated steel after oxidation in air at 800 °C. In addition, the phase structure of the oxide scale formed after 1 week was similar to that after 3 weeks, indicating that the oxide scale was stable during the oxidation time from the first week to the third week.

The surface morphologies of the uncoated and coated steels after oxidation of 3 weeks in air at 800 °C are shown in Fig. 6. The inserted are higher magnitude images from the square zone in Fig. 6a and b, respectively. The surface oxide scale formed on the uncoated steel was relatively uniform except some areas with crack and severe spallation, while the surface oxide scale developed on the Fe–Ni alloy coated steel was not uniform with some ridge-like mounds. Small flakes in Fig. 6b were observed most likely due to slight spallation from the ridge-like mounds. From the inserted higher magnitude images, it can be seen that the surface scale morphology

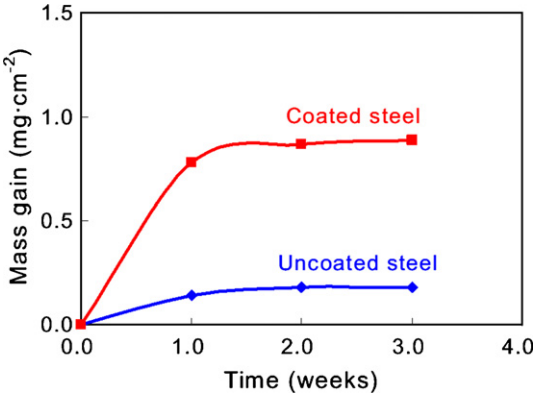

Fig. 4. Oxidation kinetics of Fe–Ni alloy coated and uncoated steels in air at 800 °C.

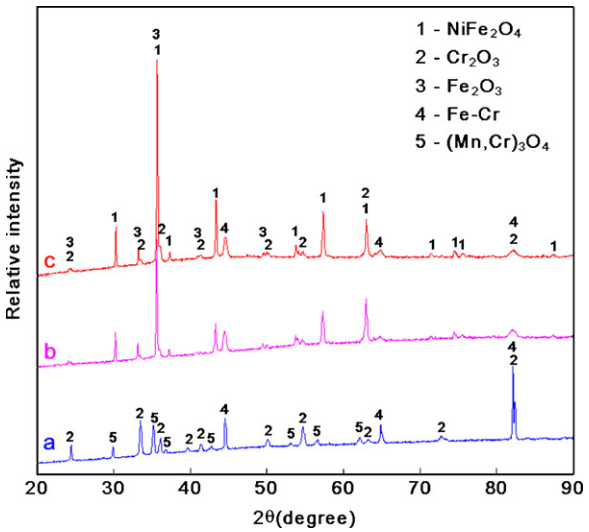

Fig. 5. XRD patterns of the oxide scale formed on uncoated and coated steels after oxidation in air at 800 °C: (a) uncoated steel oxidized for 3 weeks; (b) coated steel oxidized for 1 week; (c) coated steel oxidized for 3 weeks.

of the coated steel is completely different from that of the uncoated steel. After oxidation of 3 weeks, the ridgy mounds on the coated steel surface were Fe-rich oxide by the analysis of EDX. The Fe- and Ni-rich oxide was detected in flat areas. Based on the XRD and EDX analysis, the ridge-like mounds should be Fe_2O_3, and the Fe/Ni-rich oxide should be $NiFe_2O_4$ spinel, as shown in Fig. 6b.

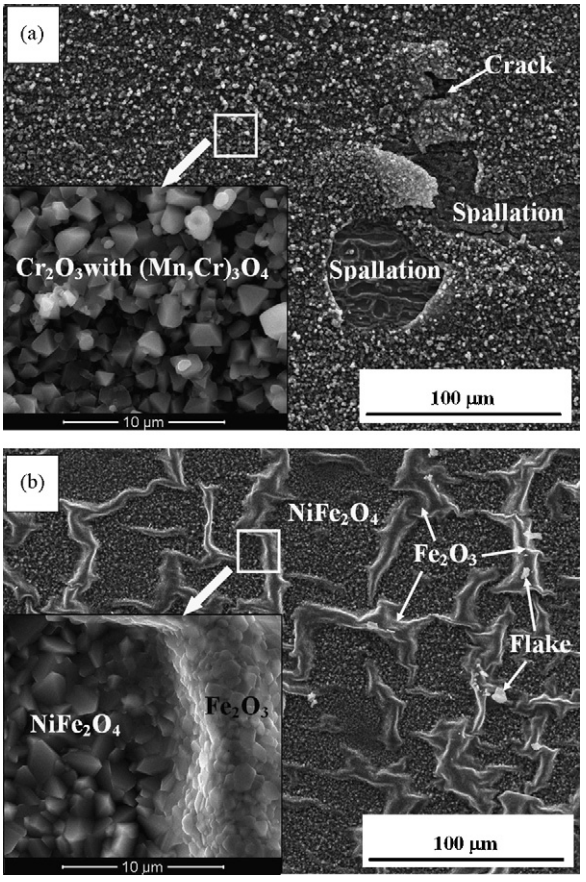

Fig. 6. SEM surface morphologies of uncoated (a) and coated (b) steels after oxidation for 3 weeks in air at 800 °C, the inserted magnitude images from the square area in (a) and (b), respectively.

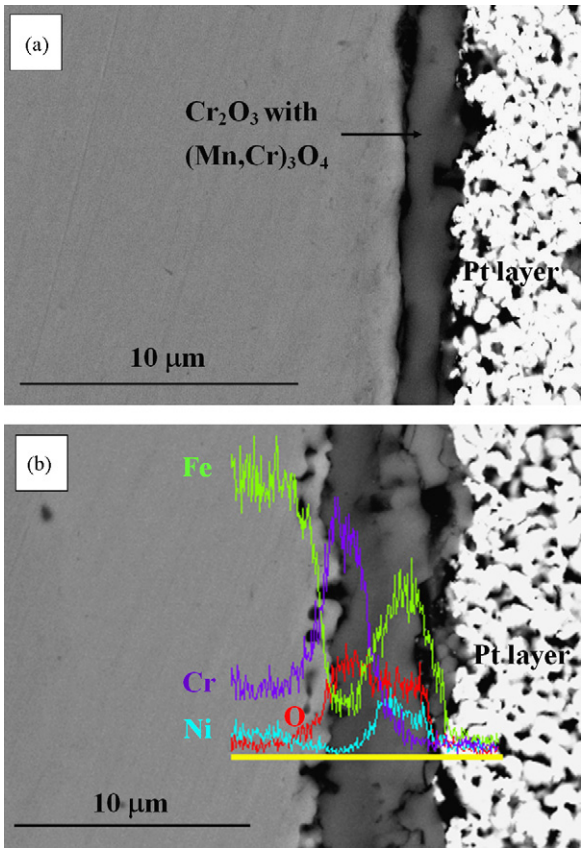

Fig. 7. Cross-section images of uncoated (a) and coated (b) steels after oxidation for 3 weeks in air at 800 °C.

The cross-section images (Fig. 7) of the coupons after a 3-week thermal exposure confirmed subsequently the difference between the oxide scales formed on the uncoated and coated steels. The oxide scale grown on the uncoated steel consisted of Cr_2O_3 with $(Mn,Cr)_3O_4$ spinel from the combined evidence of XRD and EDX, and some micro-gaps at the oxide–substrate interface were obviously observed in Fig. 7a, which might lead to cracking or severe spallation of the surface scale as indicated in Fig. 6a. In contrast, the oxide scale developed on the coated steel was comprised of a double-layer oxide structure with an outer Cr-free layer and an inner Cr-rich layer, as shown in Fig. 7b showing the cross-section microstructure with EDX line scan of the coated steel after oxidation for 3 weeks at 800 °C in air. The outer layer of the oxide scale was confirmed to be Fe- and Ni-rich oxide, and no Cr was detected. Moreover, Fe-rich oxide was detected on the scale surface, consistent with the formation of the Fe_2O_3 mounds on the oxide surface, as depicted in Fig. 6b. The inner layer was Cr-rich oxide. Based on the XRD (Fig. 5) and EDX line scan (Fig. 7b), an outer $Fe_2O_3/NiFe_2O_4$ layer atop an inner Cr_2O_3 layer was developed on the coated steel after thermal exposure. It is noted that the $NiFe_2O_4$ spinel layer appears to have improved surface scale adhesion to the steel substrate. Just a few pores at the oxide–substrate interface were observed in Fig. 7b. Furthermore, the bonding between the inner Cr_2O_3 layer and the outer $NiFe_2O_4$ spinel layer was a little too strong due to their CTE match [14,32]. The Cr_2O_3 layer with an around 2.0 μm thickness was formed on both uncoated and coated steels, indicating that the formation of the outer $NiFe_2O_4$ spinel layer did not reduce the growth rate of the inner Cr_2O_3 layer. The outer oxide layer was around 3.0–3.5 μm thick and was close to the thickness (3.0 μm) of the Fe–Ni alloy deposited on the steel, implying no severe oxide spallation for the coated steel. The Cr-free outer layer of $Fe_2O_3/NiFe_2O_4$ was converted from the Fe–Ni alloy electrodeposited on the steel substrate from which the inner layer of Cr_2O_3 was developed. It was the formation of the protective inner Cr_2O_3 layer that improved oxidation resistance of the coated steel after the initial rapid mass gain. As shown in Fig. 4, the mass gain only slightly increased with oxidation time after the first-week exposure.

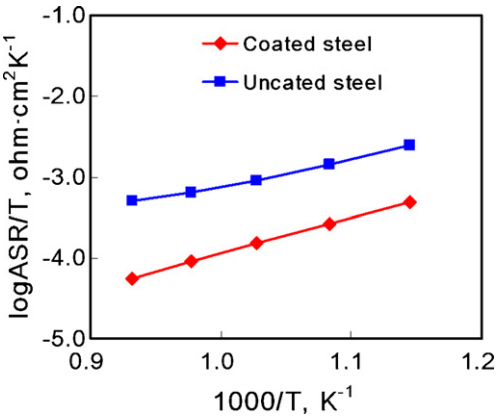

Fig. 8. Scale ASR for the coated steel after oxidation for 3 weeks in air at 800 °C, as compared to that for the uncoated steel.

3.3. Electrical properties of oxide scales

Fig. 8 shows the ASR of oxide scales developed on the uncoated and coated steels after oxidation in air at 800 °C for 3 weeks. Apparently, the scale ASR for the coated steel was lower than that of the scale for the uncoated steel, although the oxide scale (around 5.0 μm thick) formed on the coated steel was thicker than that (around 2.0 μm thick) formed on the uncoated steel. The aforementioned indicated that the thickness of Cr_2O_3 layer formed on both uncoated and coated steels was similar. The lower scale ASR for the coated steel can be attributed to the formation of the electrically conductive $Fe_2O_3/NiFe_2O_4$ outer layer [32] and subsequently reduced contact resistance between the Pt current collector and $Fe_2O_3/NiFe_2O_4$. Moreover, a significant amount of micro-gaps existed between the oxide scale and steel substrate as shown in Fig. 7a, which might increase the resistance to electrical conduction for the uncoated steel. In addition, the Cr_2O_3 layer of the coated steel could have been doped with elements from the Fe–Ni coating, thereby lowering its resistance, which needs further analysis of the two Cr_2O_3 layers from the coated and uncoated steel, respectively.

In summary, the Fe–Ni alloy is a promising candidate as Cr-free coatings on the ferritic stainless steel interconnect for intermediate-temperature SOFC, as the Cr-free $Fe_2O_3/NiFe_2O_4$ outer layer converted from the Fe–Ni alloy was electrically conductive and could suppress the evaporation of the Cr_2O_3 inner layer developed from the steel substrate. While the outer oxide layer exhibited an overall good adherence with the inner Cr_2O_3 layer after 3-week thermal exposure in air at 800 °C, further assessment should be conducted for the electrodeposited Fe–Ni alloy coatings, as the outer oxide layer did not reduce the growth rate of the inner chromia layer which could thicken, subsequently leading to cracking/spallation of the surface oxide scale or an increase in scale ASR during the long-term operation lifetime expected for the SOFC stacks.

4. Conclusion

Fe–Ni alloy was electrodeposited on the ferritic stainless steel as a method to improve high temperature electrical conductivity and to suppress the Cr evaporation. The Fe–Ni alloy was oxi-

dized to $Fe_2O_3/NiFe_2O_4$ layer beneath which Cr_2O_3 layer was thermally developed from the steel substrate in air at 800 °C. The $Fe_2O_3/NiFe_2O_4$ layer not only acted as a protective barrier to reduce the Cr evaporation, but also improved the electrical performance of the steel interconnect.

Acknowledgement

This research was sponsored by the Scientific Research Foundation for the Returned Overseas Chinese Scholars, Northeastern University, China.

References

[1] N.Q. Minh, J. Am. Ceram. Soc. 76 (1993) 563–588.
[2] B.C.H. Steele, A. Heinzel, Nature 414 (2001) 345–352.
[3] B.C.H. Steele, Solid State Ionics 134 (2000) 3–20.
[4] S.P.S. Badwal, Solid State Ionics 143 (2001) 39–46.
[5] W.Z. Zhu, S.C. Deevi, Mater. Sci. Eng. A 348 (2003) 227–243.
[6] S. de Souza, S.J. Visco, L.C. De Jonghe, J. Electrochem. Soc. 144 (1997) L35–L37.
[7] T. Ishihara, H. Matsuda, Y. Takita, J. Am. Chem. Soc. 116 (1994) 3801–3803.
[8] P. Huang, A. Petric, J. Electrochem. Soc. 143 (1996) 1644–1648.
[9] K. Huang, R.S. Tichy, J.B. Goodenough, J. Am. Ceram. Soc. 81 (1998) 2565–2575.
[10] M. Dokiya, Solid State Ionics 152 (2002) 383–392.
[11] Z. Yang, J.S. hardy, M.S. Walker, G. Xia, S.P. Simner, J.W. Stevenson, J. Electrochem. Soc. 151 (2004) A1825–A1831.
[12] J. Pu, J. Li, B. Hua, G. Xie, J. Power Sources 158 (2006) 354–360.
[13] M. Han, S. Peng, Z. Wang, Z. Yang, X. Chen, J. Power Sources 164 (2007) 278–283.
[14] S. Geng, J. Zhu, J. Power Sources 160 (2006) 1009–1016.
[15] S. Geng, J. Zhu, Z. Lu, Scr. Mater. 55 (2006) 239–242.
[16] S.P.S. Badwal, R. Deller, K. Foger, Y. Ramprakash, J.P. Zhang, Solid State Ionics 99 (1997) 297–310.
[17] Y. Matsuzaki, I. Yasuda, Solid State Ionics 132 (2000) 271–278.
[18] K. Hilpert, D. Das, M. Miller, D.H. Peck, R. Weiβ, J. Electrochem. Soc. 143 (1996) 3642–3647.
[19] S.C. Paulson, V.I. Birss, J. Electrochem. Soc. 151 (2004) A1961–A1968.
[20] S. Taniguchi, M. Kadowaki, H. Kawamura, T. Yasuo, Y. Akiyama, Y. Miyaki, T. Saitoh, J. Power Sources 55 (1995) 73–79.
[21] Y. Matsuzaki, I. Yasuda, J. Electrochem. Soc. 148 (2001) A126–A131.
[22] J.Y. Kim, V.L. Sprenkle, N.L. Canfield, K.D. Meinhardt, L.A. Chick, J. Electrochem. Soc. 153 (2006) A880–A886.
[23] S.P. Jiang, J.P. Zhang, X.G. Zheng, J. Eur. Ceram. Soc. 22 (2002) 361–373.
[24] J.H. Kim, R.H. Song, S.H. Hyun, Solid State Ionics 174 (2004) 185–191.
[25] K. Fujita, K. Ogasawara, Y. Matsuzaki, T. Sakurai, J. Power Sources 131 (2004) 261–269.
[26] Z. Yang, G. Xia, G.D. Maupin, J.W. Stevenson, Surf. Coat. Technol. 201 (2006) 4476–4483.
[27] Z. Yang, G. Xia, G.D. Maupin, J.W. Stevenson, J. Elecrochem. Soc. 153 (2006) A1852–A1858.
[28] X. Chen, P.Y. Hou, C.P. Jacobson, S.J. Visco, L. De Jonghe, Solid State Ionics 176 (5–6) (2005) 425–433.
[29] Z. Yang, G. Xia, S.P. Simner, J.W. Stevenson, J. Elecrochem. Soc. 152 (2005) A1896–A1901.
[30] J. Wu, Y. Jiang, C.D. Johnson, X. Liu, J. Power Sources 177 (2008) 365–376.
[31] J. Wu, C.D. Johnson, Y. Jiang, R.S. Gemmena, X. Liu, Electrochim. Acta 54 (2008) 793–800.
[32] J. Zhu, S. Geng, Z. Lu, W.D. Porter, J. Electrochem. Soc. 154 (2007) B1288–B1294.
[33] S. Geng, Y. Li, D. Xiang, S. Zhou, Trans. Nonferr. Met. Soc. China, in press.